13th World Conference on Earthquake Engineering
Vancouver, B.C., Canada
August 1-6, 2004
Paper No. 3189

A FRICTION DAMPER FOR POST-TENSIONED PRECAST CONCRETE BEAM-TO-COLUMN JOINTS

Brian G. MORGEN[1] and Yahya C. KURAMA[2]

SUMMARY

This paper describes an integrated experimental and analytical research program on the development of a new type of friction damper for unbonded post-tensioned precast concrete building moment frame structures in seismic regions. Previous research has shown that these structures have desirable seismic characteristics such as a self-centering capability and an ability to undergo large nonlinear lateral displacements while sustaining little damage; however, the displacements during a severe earthquake may be larger than acceptable. To reduce the seismic displacement demands, the proposed friction dampers are placed locally at selected beam-to-column joints of a frame, and dissipate energy through the displacements that occur as a result of gap opening between the precast beam and column members. Large scale beam-column specimens with and without dampers were tested under reversed cyclic loading. In addition, isolated friction damper tests were performed to evaluate the effects of dynamic loading rate on the damper behavior. The results show that the dampers can be designed to provide a significant amount of supplemental energy dissipation to a frame, while the self-centering capability of the structure is preserved. The dampers also reduce the beam deterioration under cyclic lateral loading. The experimental results are used to develop an analytical model for friction-damped precast frames.

INTRODUCTION

Precast concrete construction results in cost-effective structures that provide high quality production with minimal construction time. However, the use of precast concrete buildings in seismic regions of the United States has been limited due to uncertainty about their performance under earthquakes. In the absence of prescriptive seismic design provisions for precast concrete, current model building codes (e.g., ACI [1]) require that precast structures in seismic regions emulate the behavior of monolithic cast-in-place reinforced concrete structures, unless certain acceptance criteria (ACI [2]) are satisfied through substantial experimental and analytical evidence.

In recent years, largely through the support of the National Science Foundation (NSF), the National Institute of Standards and Technology (NIST), and the Precast/Prestressed Concrete Institute (PCI), a

[1] Graduate Research Assistant, Department of Civil Engineering and Geological Sciences, University of Notre Dame, Notre Dame, Indiana, 46556 USA.
[2] Associate Professor, Department of Civil Engineering and Geological Sciences, University of Notre Dame, Notre Dame, Indiana, 46556 USA.

significant amount of research has been conducted on the seismic behavior and design of precast concrete structures that do not emulate the behavior of cast-in-place construction. One of the "non-emulative" precast frame systems that successfully emerged from these research initiatives uses unbonded post-tensioning between the precast beam and column members to achieve the lateral load resistance needed in seismic regions (e.g., Priestley and Tao [3]; Cheok and Lew [4]; Stanton et al. [5], El-Sheikh et al. [6-8]; Priestley et al. [9]; and Stanton and Nakaki [10]).

Different from monolithic cast-in-place reinforced concrete structures, the behavior of unbonded post-tensioned precast frame structures under lateral loads is governed by the opening of gaps at the joints between the precast concrete members. In addition to significant economic benefits, these structures have desirable seismic performance characteristics such as a self-centering capability (i.e., ability to return towards the original un-displaced position upon unloading from a nonlinear lateral displacement) and an ability to undergo large nonlinear lateral displacements with little structural damage. The greatest setback to the use of unbonded post-tensioned precast frames in seismic regions is that their displacement demands during a severe earthquake may be larger than acceptable as a result of small energy dissipation (Priestley and Tao [3]). The research described in this paper focuses on this issue, with the broad objective of improving the seismic behavior of post-tensioned non-emulative precast concrete frame structures by using supplemental passive energy dissipation.

In order to reduce the lateral displacement demands during a seismic event, the use of mild steel reinforcement through the precast beam-to-column joints, in addition to the post-tensioning steel, has been investigated (e.g., Stanton et al [10]) and successfully applied in practice (Englekirk [11]). These systems are often referred to as "hybrid" precast frame systems due to the mixed use of mild steel and post-tensioning steel reinforcement. As an alternative, this paper investigates a new type of friction damper that can be used externally at selected beam-to-column joints of a frame to dissipate energy during an earthquake (see Fig. 1). The unique gap opening behavior between the beam and column members of non-emulative post-tensioned precast frames allows for the development of innovative energy dissipation systems. The proposed friction damper takes advantage of these gap opening displacements, similar to applications in post-tensioned steel frame structures (Christopoulos et al. [12]).

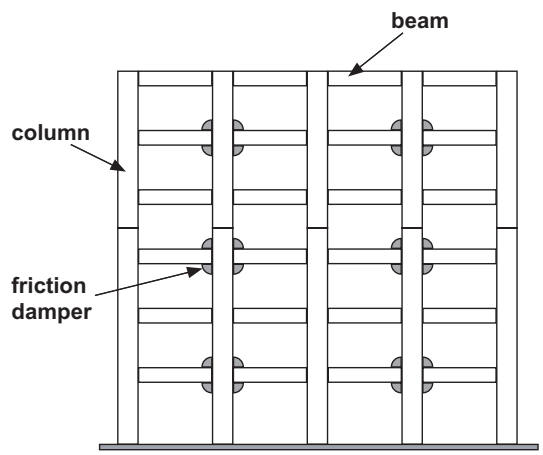

Fig. 1. Precast frame with proposed dampers.

The following sections describe the development of the proposed damper as follows. The results from a large-scale experimental research program on friction-damped beam-column subassemblies are described first. Then, a series of isolated damper tests, which were conducted to examine the effects of loading rate and slip amplitude on the damper behavior, are discussed. Finally, an analytical model that can be used to investigate the nonlinear seismic behavior of friction-damped precast concrete frames is introduced. The paper concludes with a brief summary and describes continuing research based on this research program. Complete details from the project can be found in Morgen and Kurama [13].

BEAM-COLUMN SUBASSEMBLY EXPERIMENTS

A series of large scale experiments were conducted on precast beam-column subassemblies with and without prototype friction dampers. The results from these tests, which were carried out at the University of Notre Dame's Structural Systems Laboratory, are used to evaluate the damper performance and to

determine the nonlinear behavior of frame subassemblies that use these dampers. An overview of the subassembly experimental program is given below.

Experiment Setup

A prototype unbonded post-tensioned precast concrete frame designed for a six-story office building in a region with high seismic risk (e.g., coastal California) and a site with a "medium" soil profile was selected as the basis for the beam-column subassembly experiments. This frame was adapted from El-Sheikh et al. [6-8] and is referred to as Lehigh Frame 1 in this paper. Eighty-percent scale test specimens with and without dampers were displaced under pseudo-static reversed cyclic loading. The experiment setup is shown in Figs. 2 and 3, and consists of a precast concrete test beam, oriented in a vertical configuration, and column and support fixtures. The test beam and column fixture are joined using two unbonded post-tensioning tendons and Dywidag® multi-plane anchors. Each tendon is comprised of three to seven low-relaxation ASTM A-416 strands with a nominal diameter of 0.6 in. (15.2 mm), a cross-sectional area of 0.217 in^2 (140 mm^2), and an ultimate stress of 270 ksi (1861 MPa). High strength fiber reinforced grout is used at the beam-to-column interface to provide good matching surfaces between the precast beam and the column fixture. In order to prevent bond between the strands and the concrete, the post-tensioning ducts are not filled with grout. Thus, the unbonded length of the post-tensioning steel is equal to the length of the beam specimen plus the depth of the column fixture. This length was chosen to prevent the yielding of the post-tensioning steel throughout the duration of each experiment. Note that the depth of the column fixture is larger than the scaled depth of the prototype column from Lehigh Frame 1 so as to achieve the desired unbonded length for an interior joint. More details on the test specimens and the experimental program can be found in Morgen and Kurama [13-15].

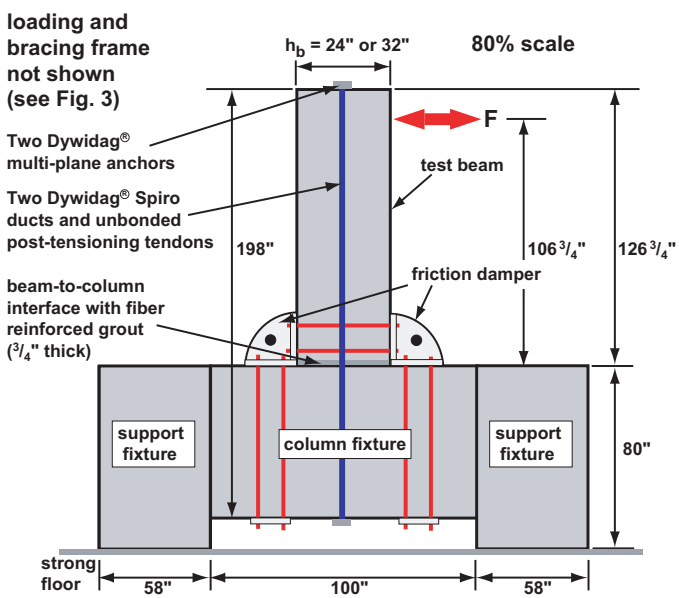

Fig. 2. Test setup. (1 in.=25.4 mm)

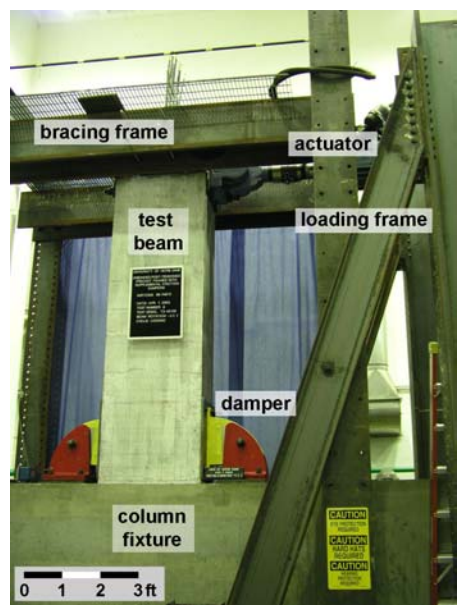

Fig. 3. Photo of test setup. (1 ft=0.3048 m)

Details of Prototype Friction Dampers

Non-emulative precast concrete frame structures are particularly suited for damage control during an earthquake. This is because, the primary mode of deformation is gap opening at the interfaces between the precast beam and column members while the precast members themselves receive little or no damage. The friction damper that was developed by this research uses these gap opening displacements to provide supplemental passive energy dissipation. As depicted in Fig. 1, the goal is to design a device that not only provides adequate energy dissipation, but also one that is easy to install, inspect, and is not intrusive to the structural layout like cross-bracing, which may be aesthetically, architecturally, and functionally undesirable.

The proposed dampers use the friction developed between adjacent metallic surfaces as gaps open and close at the beam-to-column interfaces in an unbonded post-tensioned precast frame. With the Steel Founders' Society of America (SFSA) providing assistance with cast-steel design, two pairs of prototype dampers were developed and manufactured for concept verification and for use in large-scale subassembly testing. Fig. 4(a) shows a prototype damper installed at the test beam-to-column joint. Each damper is comprised of five cast-steel components with four friction interfaces sandwiched in-between. Two of the damper components are connected to the beam while the remaining three components are connected to the column. The friction interfaces are prestressed using a 1-1/4 in. (31.8 mm) diameter A-490 structural bolt and disc spring washers as shown in Figs. 4(a) and 4(b). The spring washers help maintain a constant normal force acting on the friction interfaces as slip occurs. During testing, gap opening displacements at the beam-to-column interface result in slip displacements at the friction surfaces between the beam and column damper components, thus dissipating energy. An oversized slot shape is machined into the damper components connected to the beam to allow the slip displacements to occur [Fig. 4(c)]. The damper-to-beam and damper-to-column connections are achieved by clamping the damper components to connection plates on opposite sides of a precast member together using through bolts threaded at each end. The damper connection plates are used for construction tolerances and for the distribution of the damper forces to the beam.

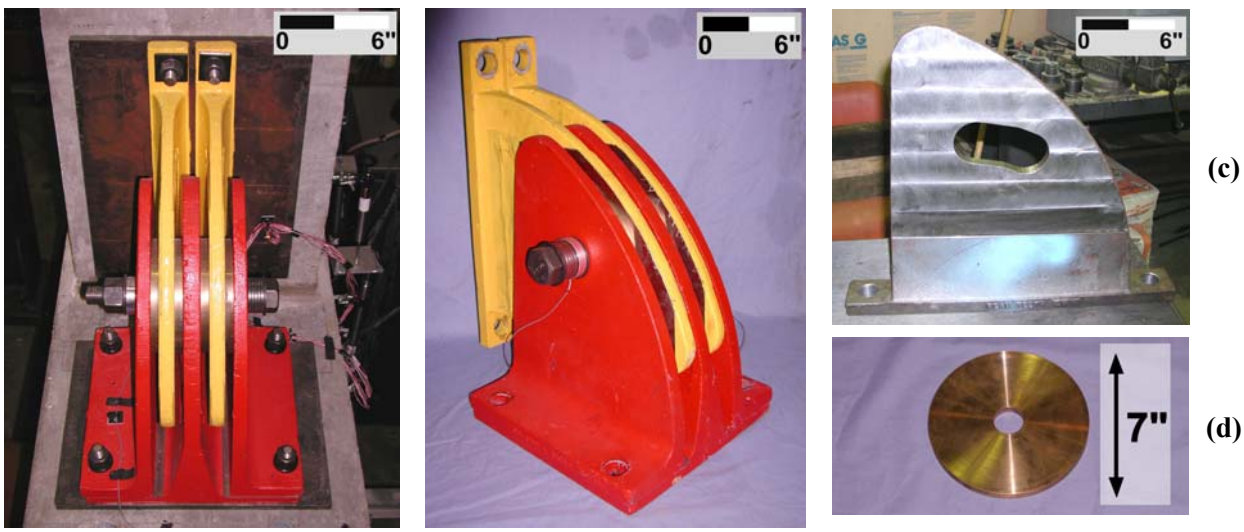

(a) (b) (c) (d)

Fig. 4: Prototype damper details – (a) beam-to-column joint; (b) damper; (c) damper component that connects to the beam; (d) leaded-bronze disc. (1 in.=25.4 mm)

Knowledge gained from past investigations of friction dampers in structural applications (e.g., Grigorian et al. [16]; Way [17]) led to the use of two types of friction interfaces in this research: (1) leaded-bronze against stainless steel; and (2) leaded-bronze against alloy steel. These configurations were previously shown to provide consistent and repeatable damper slip force-displacement characteristics. In one of the damper pairs, thin gauge [18 gauge, 0.048 in. (1.22 mm) thick] stainless steel sheets are attached with epoxy to both surfaces of the damper components connected to the beam. These tests are designated as the LB-SS (leaded-bronze against stainless steel) friction interface type. The remaining tests, using the second pair of dampers with leaded-bronze surfaces acting directly against machined cast-steel (ASTM A216 Gr. WCB) damper surfaces (with no stainless steel sheets) as shown in Fig. 4(c), are designated as the LB-CS friction interface type. The leaded-bronze surfaces at the friction interfaces are created by sandwiching 1/2 in. (12.7 mm) thick leaded-bronze (CDA 932/SAE 660 bearing bronze) discs, shown in Fig. 4(d), between the beam and column damper components.

The proposed friction damper system may have several advantages in construction to other systems, such as the hybrid system described earlier (e.g., Stanton et al [10]). One possible shortcoming of the hybrid system is the field installation of the energy dissipating mild steel reinforcement. In comparison, the proposed damper system utilizes relatively simple connections to the beam and column members; thus, possibly requiring less construction labor to install as compared to the field placement, wrapping, and grouting of the mild steel reinforcement in the hybrid system. In addition to the simpler installation, the use of the proposed damper may offer other benefits, such as: (1) post-earthquake inspections and repair (if needed) of the beam-to-column joints can be easily completed since the dampers are placed external to the joint; (2) the dampers can act as corbels to support the beams during construction, until the post-tensioning force is applied; (3) the dampers contribute to the transfer of shear forces at the beam-to-column interfaces; (4) the dampers contribute to the moment resistance at the beam ends; and (5) the damper connection plates act to confine the concrete in the beam and column members, thus, significantly reducing the deterioration of the beam ends under cyclic loading and the need to provide heavy confinement inside the concrete at the beam ends.

Testing Program

Six series of beam-column subassembly tests (a total of 55 reversed cyclic tests) using six precast concrete beam specimens were conducted with the following design parameters varied: (1) damper normal force; (2) type of friction interface; (3) area of beam post-tensioning steel; (4) initial stress of beam post-tensioning steel, and (5) beam depth. A new beam was used in the first test of each series of tests, with the displacement loading history as shown in Fig. 5 (where the beam chord rotation, θ_b, is calculated as the lateral displacement of the beam at the actuator level divided by the height to the beam-to-column interface). This beam was reused in the subsequent tests of the same series, under the same displacement history shown in Fig. 5, but with only one cycle of loading at each displacement amplitude (since little or no additional damage was observed in the test specimens following the first cycle of loading to a given displacement amplitude). Close to 100 channels of instrumentation were used in each test, including: (1) load cells to measure the total beam post-tensioning forces and the normal forces applied to the friction dampers; (2) linear displacement transducers to measure the relative displacements and deformations of the precast test specimens and fixtures; and (3) strain gauges to measure the strains in the beam and column confined concrete, beam reinforcement, and damper components. The load cells measuring the forces in the post-tensioning tendons were placed between the column fixture and the post-tensioning anchors at the bottom of the fixture. The load cells measuring the forces in the damper normal bolts were placed between the disc spring washers and the damper.

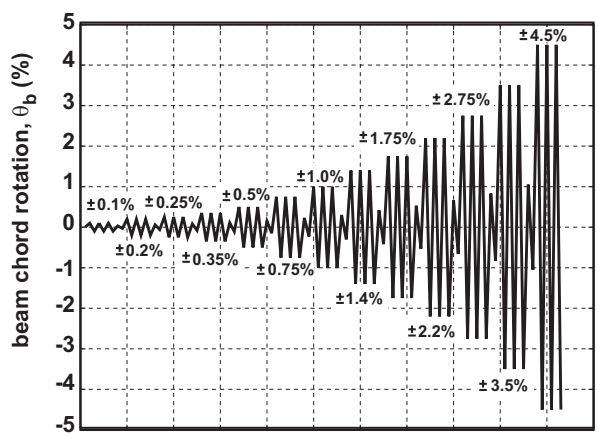

Fig. 5: Displacement loading history.

The number of post-tensioning strands used in each test, with the maximum for any test being a total of fourteen (two seven-strand groupings), is shown in Table 1. In order to account for the increase in the beam end moment resistance due to the dampers, the total post-tensioning steel area used in Test Series 1 and 2 corresponds to approximately 2/3 of the 80% scaled steel area used in Lehigh Frame 1 (El-Sheikh et al. [6-8]). The post-tensioning steel area is further varied in the other test series (see Table 1).

Table 1. Summary of beam-column subassembly test program

Series No.	Test No.	Beam No.	Test Designation	Beam Depth, h_b (in.)	No. of PT Strands	Total PT Area, A_p (in.^{2})	Average Initial PT Stress, f_{pi}/f_{pu}	Initial Total PT Force, P_i (kips)	Initial Beam Concrete Stress, f_{ci} (ksi)	Nominal Damper Normal Force, F_{dn} (kips)	Friction Interface*
1	1	1	T1-00-14	32	14	3.038	---	---	---	0	---
2	2	2	T2-26-14	32	14	3.038	0.50	411.5	0.67	26	LB-SS
	3	2	T2-13-14	32	14	3.038	0.42	346.2	0.56	13	LB-SS
	4	2	T2-00-14	32	14	3.038	0.42	344.8	0.56	39	LB-SS
	5	2	T2-39-14	32	14	3.038	0.42	345.3	0.56	0	LB-SS
	6	2	T2-00/52-14	32	14	3.038	0.42	346.1	0.56	varies	LB-SS
	7	2	T2-00|00/39-14	32	14	3.038	0.42	347.3	0.57	varies	LB-SS
3	8	3	T3-26-06	32	6	1.302	0.66	232.2	0.38	26	LB-SS
	9	3	T3-00-06	32	6	1.302	0.59	206.0	0.34	0	---
	10	3	T3-13-06	32	6	1.302	0.59	208.0	0.34	13	LB-SS
	11	3	T3-26b-06	32	6	1.302	0.59	205.8	0.33	26	LB-SS
	12	3	T3-39-06	32	6	1.302	0.59	208.7	0.34	39	LB-SS
	13	3	T3-26-10	32	10	2.170	0.52	305.3	0.50	26	LB-SS
	14	3	T3-00-10	32	10	2.170	0.50	294.2	0.48	0	---
	15	3	T3-13-10	32	10	2.170	0.49	289.8	0.47	13	LB-SS
	16	3	T3-39-10	32	10	2.170	0.49	289.8	0.47	39	LB-SS
	17	3	T3-52-10	32	10	2.170	0.50	292.7	0.48	52	LB-SS
	18	3	T3-26-14	32	14	3.038	0.57	470.4	0.77	26	LB-SS
	19	3	T3-00-14	32	14	3.038	0.56	456.2	0.74	0	---
	20	3	T3-13-14	32	14	3.038	0.55	454.7	0.74	13	LB-SS
	21	3	T3-39-14	32	14	3.038	0.55	453.2	0.74	39	LB-SS
	22	3	T3-52-14	32	14	3.028	0.56	456.2	0.74	52	LB-SS
4	23	4	T4-26-06	32	6	1.302	0.56	197.2	0.32	26	LB-CS
	24	4	T4-00-06	32	6	1.302	0.38	131.9	0.21	0	---
	25	4	T4-13-06	32	6	1.302	0.37	129.5	0.21	13	LB-CS
	26	4	T4-26b-06	32	6	1.302	0.37	128.5	0.21	26	LB-CS
	27	4	T4-39-06	32	6	1.302	0.37	129.2	0.21	39	LB-CS
	28	4	T4-26-10	32	10	2.170	0.48	280.6	0.46	26	LB-CS
	29	4	T4-00-10	32	10	2.170	0.45	262.8	0.43	0	---
	30	4	T4-13-10	32	10	2.170	0.45	262.5	0.43	13	LB-CS
	31	4	T4-26b-10	32	10	2.170	0.45	261.8	0.43	26	LB-CS
	32	4	T4-39-10	32	10	2.170	0.45	262.2	0.43	39	LB-CS
	33	4	T4-52-10	32	10	2.170	0.45	261.8	0.43	52	LB-CS
	34	4	T4-65-10	32	10	2.170	0.45	262.8	0.43	65	LB-CS
	35	4	T4-26-14	32	14	3.038	0.52	425.9	0.69	26	LB-CS
	36	4	T4-00-14	32	14	3.038	0.52	423.3	0.69	0	---
	37	4	T4-13-14	32	14	3.038	0.51	420.3	0.68	13	LB-CS
	38	4	T4-26b-14	32	14	3.038	0.51	419.9	0.68	26	LB-CS
	39	4	T4-39-14	32	14	3.038	0.51	419.9	0.68	39	LB-CS
	40	4	T4-52-14	32	14	3.028	0.51	419.2	0.68	52	LB-CS
	41	4	T4-65-14	32	14	3.028	0.51	419.2	0.68	52	LB-CS
	42	4	T4-65b-14	32	14	3.038	0.51	418.9	0.68	65	LB-CS
5	43	5	T5-00-14	32	14	3.038	0.51	416.5	0.68	0	---
6	44	6	T6-65-14A	24	14	3.038	0.38	307.7	0.67	65	LB-CS
	45	6	T6-00-14A	24	14	3.038	0.35	287.4	0.62	0	---
	46	6	T6-13-14A	24	14	3.038	0.35	285.7	0.62	13	LB-CS
	47	6	T6-26-14A	24	14	3.038	0.35	285.4	0.62	26	LB-CS
	48	6	T6-39-14A	24	14	3.038	0.35	285.4	0.62	39	LB-CS
	49	6	T6-52-14A	24	14	3.038	0.35	284.4	0.62	52	LB-CS
	50	6	T6-65-14B	24	14	3.038	0.51	420.4	0.91	65	LB-CS
	51	6	T6-00-14B	24	14	3.038	0.49	405.7	0.88	0	---
	52	6	T6-13-14B	24	14	3.038	0.49	401.5	0.87	13	LB-CS
	53	6	T6-26-14B	24	14	3.038	0.49	400.5	0.87	26	LB-CS
	54	6	T6-39-14B	24	14	3.038	0.49	399.4	0.87	39	LB-CS
	55	6	T6-52-14B	24	14	3.038	0.49	398.0	0.86	52	LB-CS

* LB-SS = Leaded-Bronze against Stainless Steel
LB-CS = Leaded-Bronze against Machined Cast-Steel Damper Surface

** 1 in. = 25.4 mm; 1 kip = 4.448 kN; 1 ksi = 6.895 MPa.

Overall Test Specimen Response

The overall behavior from the beam-column subassembly experiments without and with dampers (Tests 43 and 35) is illustrated in Figs. 6(a) and 6(b), respectively. In both types of experiments, the beams behaved as expected and designed. As the actuator was displaced at the top, the beam responded similar to a rigid member with most of the nonlinear deformation occurring as a result of gap opening at the beam-to-column interface. The restoring effect of the post-tensioning force resulted in a self-centered behavior, closing the gap and reversing the slip displacements in the dampers upon unloading.

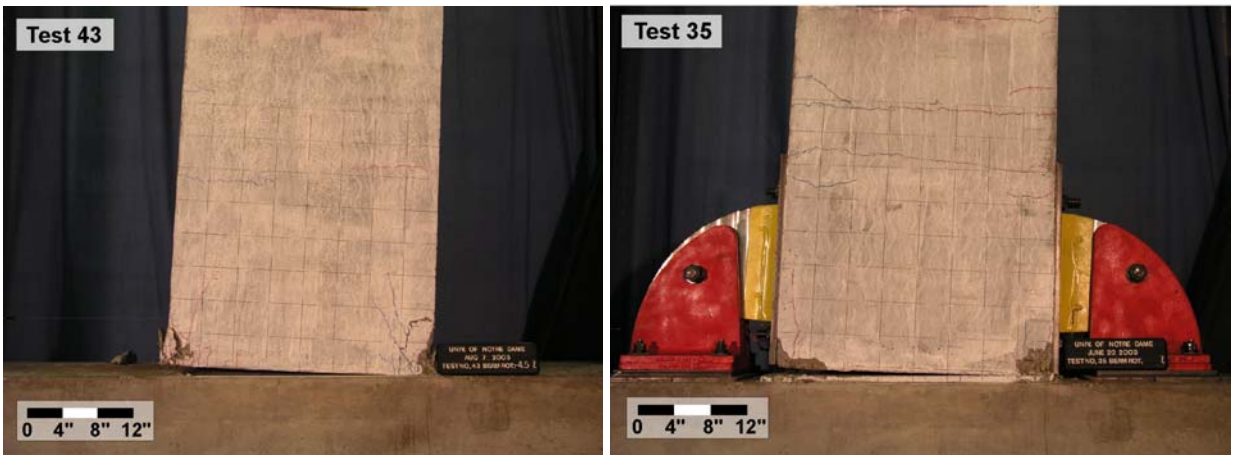

(a) **(b)**

Fig. 6: Displaced position of beam – (a) without dampers; (b) with dampers. (1 in.=25.4 mm)

The experiments without dampers (Test Series 1 and 5; see Table 1) were used as a baseline for comparison with the experiments that included friction dampers (Test Series 2, 3, 4, and 6). As an example, Figs. 7(a) and 7(b) show the hysteretic beam end moment (M_b) versus beam chord rotation (θ_b) results from a baseline test with no dampers (Test 43) and from a test with friction dampers (Test 44), respectively. The beam end moment, M_b, is calculated as the actuator force multiplied by the height to the beam-to-column interface and the beam chord rotation, θ_b, is calculated as the beam lateral displacement at the actuator level divided by the height to the beam-to-column interface. It can be seen from the hysteresis loops in Fig. 7(a) that the specimen without dampers behaves essentially elastic through nonlinear displacements (i.e., nonlinear-elastic), with very little energy dissipation but extremely good self-centering capability. As shown in Fig. 7(b), the energy dissipation of the specimen can be significantly increased by using the proposed friction dampers, while preserving the desired self-centering capability. Note that the hysteresis loops in Fig. 7(b) correspond to a beam with a smaller depth [h_b=24 in. (610 mm)] than the beam in Fig. 7(a) [h_b=32 in. (813 mm); see Table 1]. The results show that the maximum moment resistance of the smaller beam with dampers is larger that the resistance of the deeper beam without dampers. It is concluded that the proposed friction dampers contribute significantly to the beam end moment resistance, which may lead to the design of smaller beams in practice.

Damper Normal Force

This section describes the effect of the damper normal force, F_{dn}, on the hysteretic beam end moment versus chord rotation relationship from the subassembly experiments. The six different hysteresis loops in Fig. 8(a) correspond to a beam chord rotation of θ_b=±4.5% for the same test beam (Beam 6), the same total initial post-tensioning force, P_i, and the same friction interface type (LB-CS), but with varying levels of the damper normal force (Tests 44-49). Note that the results from the third cycle of loading to θ_b=±4.5% are shown for the virgin beam (Test 44).

The results indicate that the inelastic energy dissipation per loading cycle, which can be calculated as the shaded area enclosed by the hysteresis loop during that cycle, D_h, gets larger as the damper normal force is increased (assuming that the friction interface type is kept the same). The results from the experiments without and with dampers are evaluated for conformance to the *ACI T1.1-01* Standard (ACI [2]). According to *ACI T1.1-01*, the smallest acceptable value for the relative energy dissipation ratio (β) is specified as 0.125. The *relative energy dissipation ratio* is defined for a beam moment-rotation cycle as the ratio of the area D_h enclosed by the hysteresis loop for that cycle [shaded areas in Fig. 8(a)] to the area of the circumscribing parallelogram. The circumscribing area [dashed lines in Fig. 8(a)] is defined by the initial stiffnesses measured during the first linear-elastic cycle of loading and the peak positive and negative moment resistances during the cycle for which the relative energy dissipation ratio is calculated (ACI [2]). The relative energy dissipation ratio, β, is a measure of the amount of viscous damping in an equivalent linear-elastic system that would result in the same amount of energy dissipation as the nonlinear system. The *ACI T1.1-01* Standard recommends that if β is smaller than 0.125, there may be inadequate damping for the frame as a whole, and the oscillations of the frame may continue for a considerable time after an earthquake, possibly producing low-cycle fatigue effects and excessive displacements.

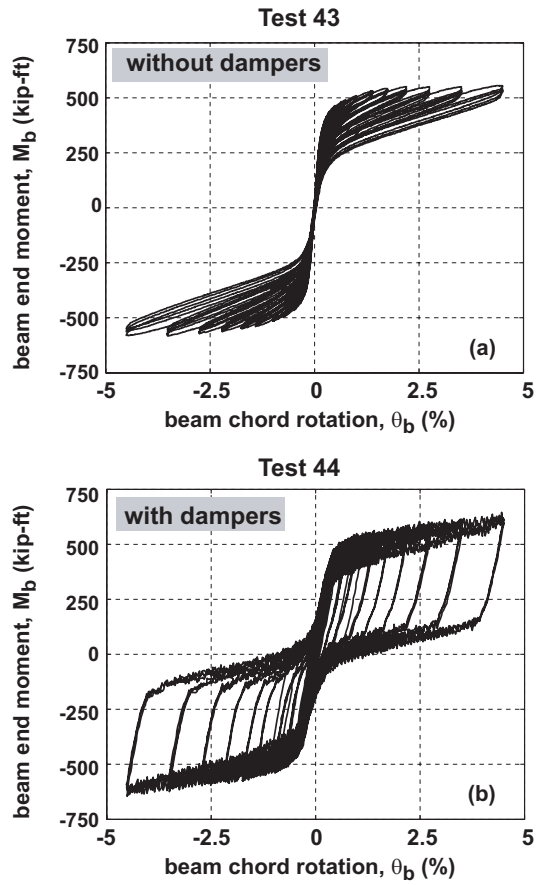

Fig. 7: M_b-θ_b – (a) without dampers; (b) with dampers. (1 kip=4.448 kN; 1 ft=0.3048 m)

Fig. 8(b) illustrates the effect of the friction dampers on the relative energy dissipation ratio of the specimens from Tests 44 to 49 corresponding to a beam chord rotation of θ_b=±4.5%. The test specimen with no dampers [Fig. 8(a); F_{dn}=0 kips] shows unacceptable behavior (with β<0.125) while the specimens with damper normal force, F_{dn}, larger than approximately 20 kips (89 kN) have acceptable behaviors (with β>0.125) and also meet all of the other prescriptive acceptance requirements of *ACI T1.1-01* (ACI [2]). Looking at the plot in Fig. 8(b), it can be observed that as the damper normal force is increased (i.e., damper slip force increased), the relative energy dissipation ratio increases nearly proportionally.

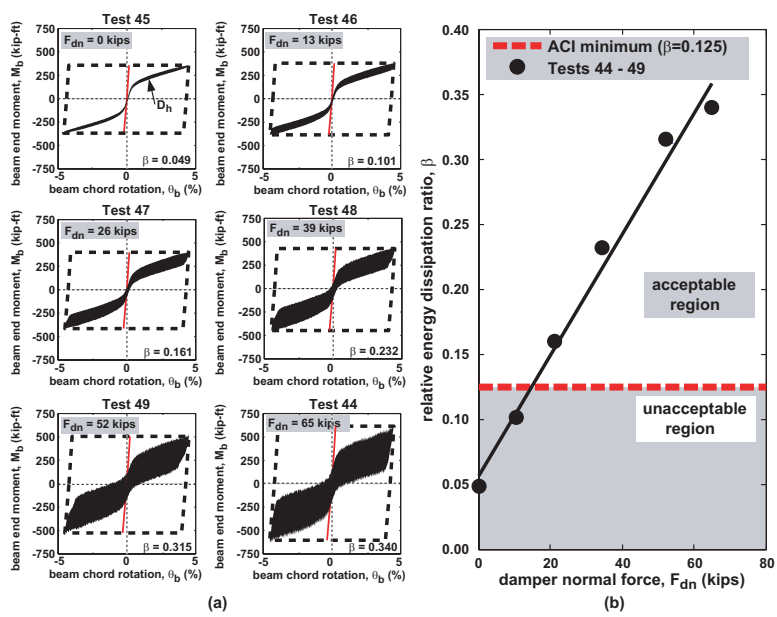

Fig. 8: Effect of damper normal force – (a) hysteresis loops; (b) relative energy dissipation ratio. (1 kip=4.448 kN; 1 ft=0.3048 m)

Beam Deterioration

One of the desirable effects of the proposed friction damper on the beam-column subassembly behavior is a significant reduction in the observed beam deterioration. Since the damper-to-beam connections are achieved by clamping two dampers on opposite sides of the beam together using through bolts threaded at each end, the damper connection plates [see Figs. 4(a) and 6(b)] confine the concrete at the beam ends. This concrete confinement helps to reduce the beam deterioration that occurs throughout the cyclic displacement loading history, and may reduce the need to provide heavy confinement inside the concrete at the beam ends. Furthermore, the proposed damper, which contributes significantly to the beam end moment resistance as shown previously, has non-deteriorating force-displacement characteristics.

As an example, Fig. 9 shows the measured beam end moment versus chord rotation relationships from Test 43 (without dampers) and Test 2 (with dampers). Both of these specimens are 32 in. (813 mm) deep virgin beams with similar average initial post-tensioning stress, f_{pi}, and similar initial concrete stress, f_{ci}, as shown in Table 1. For each test, the last moment-rotation hysteresis loop to θ_b=±3.5% (shaded area) is compared with the entire hysteretic behavior (thin light lines). It can be observed that the differences in resistance and stiffness between the envelope curve and the last hysteresis loop of the specimen without dampers (Test 43) are much larger than the differences for the friction-damped specimen (Test 2), thus, demonstrating the reduced deterioration due to the use of the dampers.

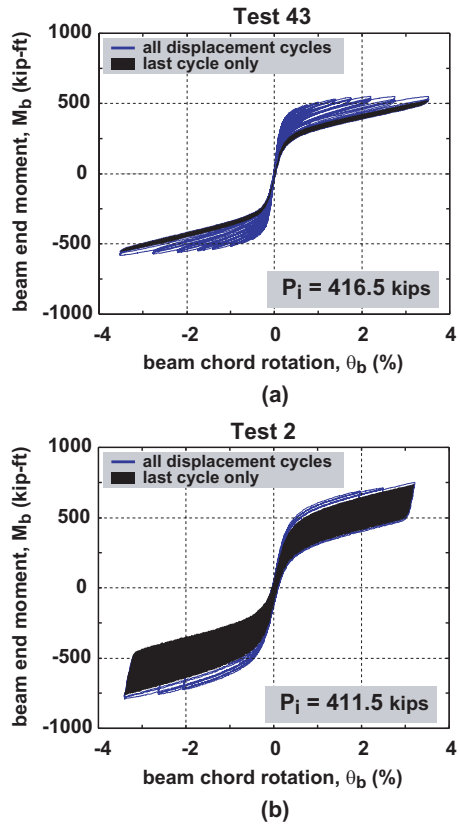

Fig. 9: Beam deterioration – (a) without dampers; (b) with dampers. (1 kip=4.448 kN; 1 ft=0.3048 m)

ISOLATED DAMPER EXPERIMENTS

Using the pseudo-static beam-column subassembly tests described above, the coefficient of friction for the prototype dampers was determined to be in the range of 0.17 to 0.22. These values are within ranges reported by previous research (Way [17]). In order to supplement the beam-column subassembly results, additional isolated damper experiments were conducted to determine the effect of dynamic loading displacement rate and amplitude on the damper behavior. The objectives of these experiments were: (1) direct measurement of the coefficient of friction for the two different friction interfaces (LB-SS and LB-CS) used in the prototype dampers; (2) direct evaluation of the damper force-displacement behavior; and (3) direct evaluation of the damper force-velocity relationships. The following sections describe the isolated friction damper experiments in more detail and present selected results.

Experiment Setup

The isolated damper experiment setup is depicted in Figs. 10 and 11. As seen in the test photo in Fig. 10, the loading system includes a 55 kip (245 kN) 10 in. (254 mm) stroke dynamic-rated actuator that is configured with a 100-gpm (379 lit/min) Moog servo-valve, a 166-gpm (628 lit/min) Hydraulic Control Module, and a 90-gpm (341 lit/min) capacity hydraulic pump. The system is controlled by a Schenck-Pegasus 5910 servo-hydraulic controller in displacement feedback mode. With these specifications, a wide range of frequencies and slip amplitudes (e.g., ±2 in. at 2 Hz) can be imposed to the friction interface. The actuator has internal load cell and displacement transducers, which are used to measure the

actuator forces and displacements. An additional displacement transducer (LVDT) is placed locally at the friction interface to capture the slip displacements that occur directly at the interface.

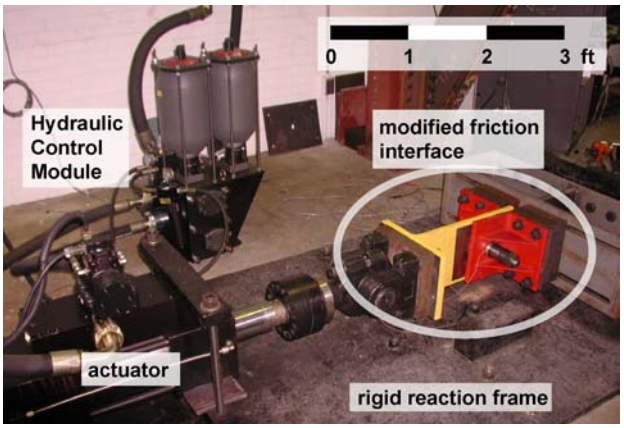

Fig. 10: Photo of isolated damper test region. (1 ft=0.3048 m)

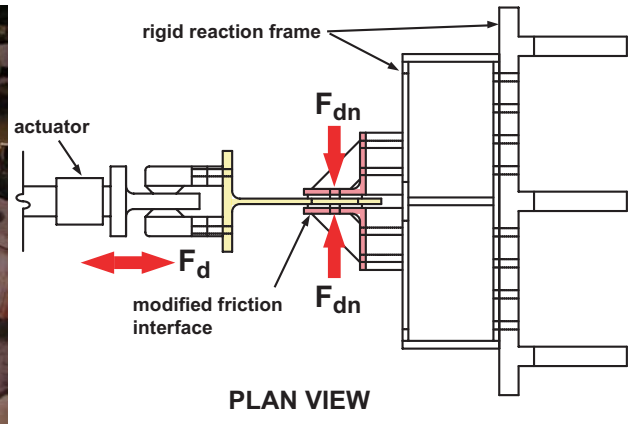

Fig. 11: Detail of isolated damper test setup.

The friction damper is inserted into a "rigid" reaction frame, in line with the hydraulic actuator. The isolated damper experiments impose linear translational displacements to the friction damper interface. Since the prototype dampers from the beam-column subassembly experiments translate and rotate, a modified friction damper (see Fig. 10) was manufactured for use in the linear actuator reaction frame. The modified linear damper model is comprised of three components with two friction interfaces sandwiched in-between. Dampers with both types of friction interfaces from the beam-column subassembly tests were developed; namely the LB-SS and LB-CS friction interface types. The two linear damper components that model the column components from the prototype friction damper are attached to the rigid reaction frame as shown in the detail drawing of the isolated damper test region in Fig. 11. The linear damper component that simulates the beam components of the prototype friction damper is directly attached to the actuator. The friction interfaces are prestressed using a 1-1/4 in. (31.8 mm) diameter A-490 structural bolt and disc spring washers to the same nominal damper normal force levels used in the friction dampers from the beam-column subassembly experiments. Similar to the subassembly prototype dampers, the disc spring washers help maintain a constant normal force acting on the friction interfaces as slip occurs. Note that since the linear damper model consists of two friction interfaces, whereas the prototype friction damper from the subassembly experiments contain four, the slip forces associated with the linear damper are approximately half as much as the prototype damper.

Testing Program

In order to investigate the effect of dynamic loading displacement rate and amplitude on the damper behavior, a series of force-displacement tests under triangular displacement excitation were conducted. Since the triangular displacement waveform does not introduce inertial forces into the system, except when the constant velocity changes its direction, this type of test allows for a more direct measurement of the force-displacement and force-velocity relationships for the damper. As shown in Table 2, this test sequence consisted of several excitation frequencies, displacement amplitudes, and damper normal forces using the LB-SS and LB-CS friction interface models. The excitation frequencies and amplitudes were selected based on a series of nonlinear dynamic time-history analyses of multi-story prototype friction-damped precast frames. The excitation frequency of f=0.0025 Hz at an amplitude of ±0.25 in. represents the slow rate used in the pseudo-static beam-column subassembly tests described earlier.

Table 2. Triangular displacement waveform test series

Actuator Amplitude (in.)	Excitation Frequency, f (Hz)											Damper Normal Force, F_{dn} (kips)				
±1/6**	---	---	---	---	---	---	---	1.50	---	---	---	---	---	---	---	65
±0.25*	0.0025	0.10	0.25	0.50	0.75	1.00	1.25	1.50	2.00	3.00	5.00	13	26	39	52	65
±1/3**	---	---	---	---	---	---	---	1.50	---	---	---	---	---	---	---	65
±0.5**	---	---	---	0.50	---	1.00	---	---	---	---	---	---	---	---	---	65
±5/6**	---	---	---	---	---	---	---	1.50	---	---	---	---	---	---	---	65
±1.00**	---	---	---	0.50	---	---	---	---	---	---	---	---	---	---	---	65
±1.25**	---	---	---	---	---	1.00	---	---	---	---	---	---	---	---	---	65
±2.50**	---	---	---	0.50	---	---	---	---	---	---	---	---	---	---	---	65

Notes: *Both the LB-SS and LB-CS interface models are tested at this amplitude. Total number of test combinations = 2 interfaces x 1 amplitude x 11 frequencies x 5 damper normal forces = 110 tests.
**Only the LB-CS interface model is tested at these amplitudes. Total number of test combinations = 8 tests.
(1 in.=2.54 mm; 1 kip=4.448 kN)

In addition to the triangular displacement waveform tests, a series of experiments using sinusoidal displacement excitations (see Table 3) were conducted on the LB-CS friction interface. Once again, frequency-dependency tests, amplitude dependency tests, and test sequences with variable damper normal forces were conducted.

Table 3. Sinusoidal displacement waveform test series

Actuator Amplitude (in.)	Excitation Frequency, f (Hz)											Damper Normal Force, F_{dn} (kips)				
±0.25	0.0025	0.10	---	0.50	---	1.00	---	1.50	---	3.00	5.00	13	26	39	52	65
±0.50	0.0025	0.10	---	0.50	---	1.00	1.25	1.50	---	3.00	---	13	26	39	52	65
±1.00	0.0025	0.10	---	0.50	0.75	1.00	---	1.50	2.00	---	---	13	26	39	52	65
±1.75	0.0025	0.10	0.25	0.50	---	1.00	1.25	1.50	---	---	---	13	26	39	52	65

Note: Only the LB-CS interface model is tested under the sinusoidal displacement waveform. Total number of test combinations = 4 amplitudes x 7 frequencies x 5 damper normal forces = 140 tests. (1 in.=2.54 mm; 1 kip=4.448 kN)

Selected Results

Selected results from the triangular displacement experiments using the LB-CS friction interface type are presented in this section. Results from the other isolated damper experiments can be found in Morgen and Kurama [13]. As an example, Fig. 12(a) shows the damper force versus displacement (F_d-d) hysteresis results from a test sequence with the triangular displacement waveform as follows: increasing excitation frequency of f =0.10 to 5.00 Hz, constant excitation amplitude of ±0.25 in. (±6.35 mm), nominal damper normal force of F_{dn}=65 kips (289 kN), and leaded-bronze versus machined cast-steel (LB-CS) friction interface. Similarly, Fig. 12(b) shows the damper force versus displacement hysteresis results from a second test sequence with the triangular displacement waveform as follows: constant excitation frequency of f=1.00 Hz, constant excitation amplitude of ±0.25 in. (±6.35 mm), increasing nominal damper normal force of F_{dn}=13 to 65 kips (58 to 289 kN), and leaded-bronze versus machined cast-steel (LB-CS) friction interface. The damper force is measured using the actuator load cell and the damper displacement is measured using the transducer (LVDT) placed locally at the friction interface.

Note that the goal of the damper friction interface is not necessarily to produce the largest amount of energy dissipation possible, but rather to result in a damper that possesses a consistent and predictable response. It can be seen from Fig. 12(a) that the hysteresis plots for the wide range of excitation frequencies tested fall on top of one another and produce a stable close-to-rectangular force-displacement behavior with little or no degradation or change in the slip load. The results in Fig. 12(b) illustrate that increasing damper normal force results in an increase in the damper slip force without changing the damper dynamic characteristics. These findings from the isolated damper experiments show that the

proposed friction damper for use in unbonded post-tensioned precast concrete moment frames can provide predictable and consistent levels of supplemental energy dissipation, independent of excitation frequency and velocity.

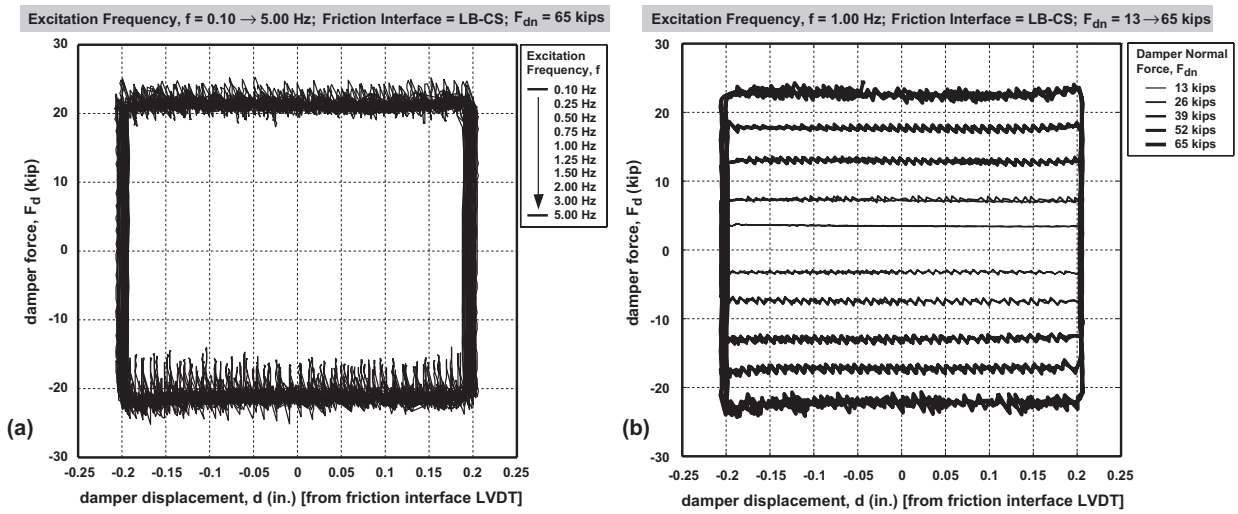

Fig. 12: Friction damper force-displacement relationships – (a) with increasing excitation frequency; (b) with increasing damper normal force. (1 kip=4.448 kN; 1 in. = 25.4 mm)

ANALYTICAL MODELING

The experimental results described above are used to develop an analytical model for post-tensioned friction-damped precast concrete beam-column subassemblies. This subassembly model is needed to investigate the behavior of multi-story friction-damped precast moment frames under earthquake-induced loads. The DRAIN-2DX structural analysis program (Parkash et al. [18]) is used as the analytical platform. More information on the analytical modeling can be found in Morgen and Kurama [13].

As described earlier, the nonlinear deformations of post-tensioned friction-damped precast concrete frames occur primarily at the beam-to-column joint regions. It is therefore important to focus on the behavior of these regions, including gap opening at the beam-to-column interfaces, joint panel zone shear deformations, inelastic behavior at the ends of the precast beam members at large rotations, and the behavior of the dampers. As shown in Fig. 13(a) for an interior beam-column subassembly, the following elements are used in the model adapted from El-Sheikh et al. [6,-8]: (1) fiber beam-column elements to model the beam and column members; (2) truss elements to model the unbonded post-tensioning steel; and (3) zero-length rotational spring elements to model the panel zone shear deformations.

Additionally, the effect of the friction dampers on the beam-column subassembly behavior is modeled using yielding truss elements with an elastic-perfectly-plastic hysteretic behavior as shown in Fig. 13(b). This analytical model is used to investigate the beam-column subassembly specimens

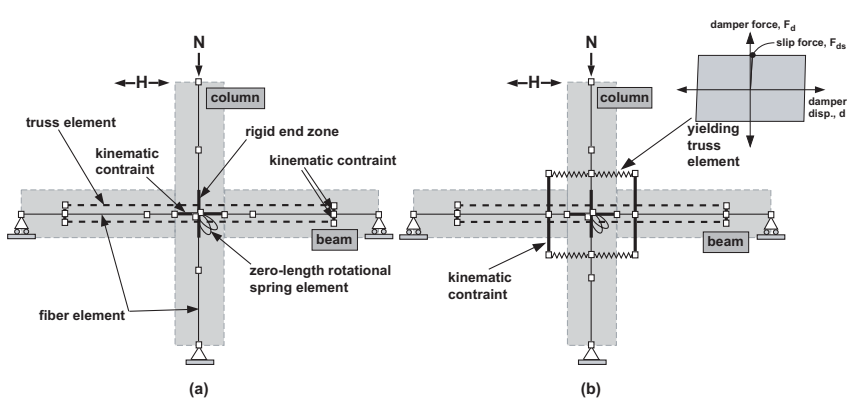

Fig. 13: Analytical model for an interior beam-column subassembly – (a) without dampers; (b) with dampers.

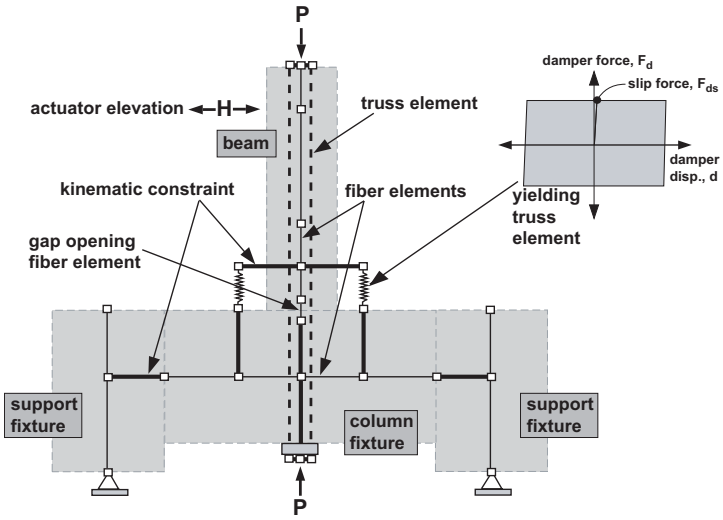

Fig. 14: Subassembly experiment verification analytical model.

as depicted in Fig. 14. Note that the close-to-rectangular force-displacement model for the friction dampers in Figs. 13(b) and 14 matches very well with the measured behavior from the isolated damper tests [see Figs. 12(a-b)].

Results from the analytical model with and without friction dampers are compared with the beam-column experiment results. As an example, the plots in Fig. 15 depict measured versus predicted behaviors from a test with friction dampers (Test 8) and a baseline test without friction dampers (Test 43). The top row of plots [Fig. 15(a)] compares the measured hysteretic beam end moment versus chord rotation behavior with the analytical results. Similarly, the bottom row of plots [Fig. 15(b)] shows comparisons for the total post-tensioning force versus beam chord rotation behavior. It can be seen that both the model without friction dampers and the model that incorporates the friction dampers through the use of simple yielding truss elements produce reasonable analytical comparisons to the experimental results. The relatively simple modeling of the proposed friction damper is an additional advantage for seismic analysis and design purposes.

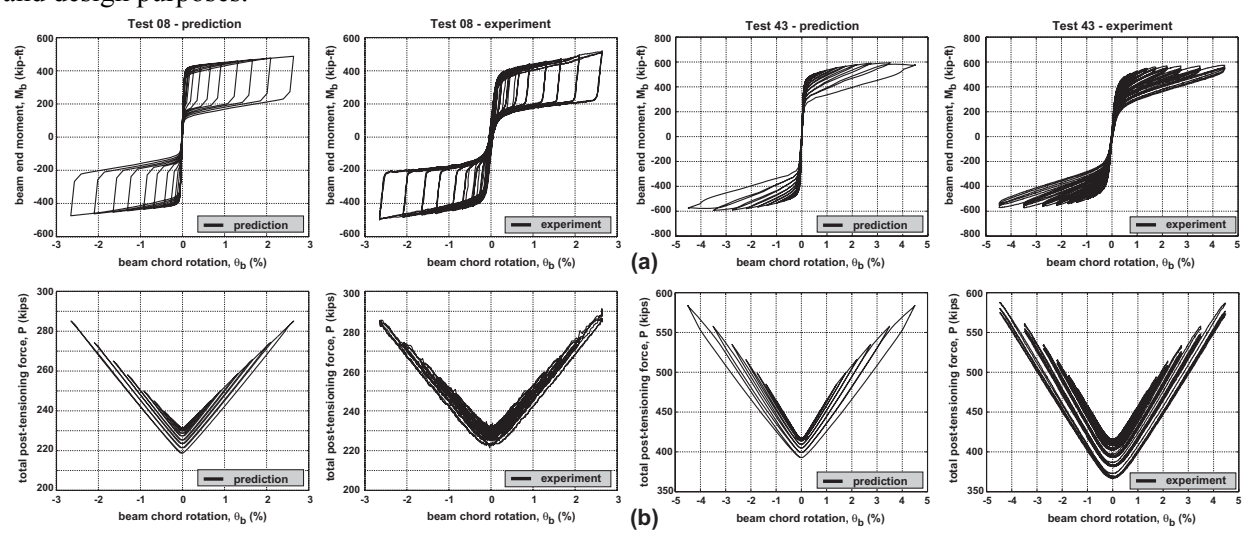

Fig. 15: Verification of the analytical model – (a) M_b-θ_b hysteresis; (b) P-θ_b hysteresis. (1 kip=4.448 kN; 1 ft = 0.3048 m)

SUMMARY, CONCLUSIONS, AND ONGOING RESEARCH

Based on the large-scale beam-column subassembly and isolated damper experiments described in this paper, the use of the proposed friction damper to increase the energy dissipation of unbonded post-tensioned precast concrete building frames in regions of high and moderate seismic risk is promising. The following advantages of the friction-damped system have been demonstrated through this research:

- In terms of construction and installation:
  (1) the dampers require a relatively simple field installation procedure;

(2) the dampers can act as corbels to support the beams during construction prior to the application of the post-tensioning force; and
(3) post-earthquake inspections and repair (if needed) of the beam-to-column joints can be easily completed since the dampers are external to the joint.

- In terms of beam-column subassembly behavior:
  (1) the dampers contribute to the transfer of shear forces at the beam-to-column interfaces;
  (2) the dampers contribute to the beam end moment resistance so smaller depth beams with dampers can have the same resistance as larger depth beams without dampers;
  (3) the dampers help to increase the amount of energy dissipation, namely the relative energy dissipation ratio, above the *ACI T1.1-01* Standard minimum (ACI [2]); and
  (4) the damper connection plates act to confine the concrete in the beam and column members, thus significantly reducing the deterioration at the beam ends under cyclic lateral loading and the need for heavy concrete confinement.
- In terms of design and analysis:
  (1) the dampers are simple to model analytically; and
  (2) the dampers provide a reliable and consistent hysteretic force-displacement response that is independent of excitation frequency and velocity.

This research program has shown that the proposed friction-damped precast concrete beam-column system is a viable and competitive structural system. Note that the goal of this project has been the concept development and verification of the new damper. Future practical applications may require further refinement of the damper components. Current research is conducting analytical investigations to determine the effects of a number of structural parameters on the seismic behavior of multi-story friction-damped precast frame structures, including: (1) frame dimensions; (2) number, location, and slip force of the friction dampers; and (3) amount of post-tensioning in the precast members. Comparisons of precast frames with and without friction dampers are being made against hybrid precast systems that use mild steel reinforcement through the beam-to-column joints and against traditional monolithic cast-in-place reinforced concrete systems. Simplified methods for analysis/design are investigated, including, representation of the multi-degree-of-freedom frame system using equivalent linear-elastic and nonlinear single-degree-of-freedom models. A design approach for the friction dampers is developed to determine the required number of dampers and the damper slip force to reduce the peak lateral displacements of the structure to below an allowable target displacement. Ultimately, the results will be used to develop performance-based seismic analysis/design tools and guidelines.

ACKNOWLEDGMENTS

This research is funded by the National Science Foundation (NSF) under Grant No. CMS 98-74872 as a part of the CAREER Program. The support of the NSF Program Directors Drs. S.C. Liu and S.L. McCabe is gratefully acknowledged. In addition, the authors recognize the technical and financial support provided by industry partnerships with: R.W. Monroe and D.R. Poweleit of the Steel Founders' Society of America; R. Reddy of Southwest Steel Casting Company of Longview, Texas; C.E. Hilgeman and M.A. Fusani of Concrete Technology, Inc. of Springboro, Ohio; and K.B. Allen and D. Martin of Dywidag-Systems International of Bolingbrook, Illinois. The opinions, findings, and conclusions expressed in this paper are those of the authors and do not necessarily reflect the views of the NSF or the individuals and organizations acknowledged above.

REFERENCES

1. ACI, Committee 318, "Building Code Requirements for Structural Concrete (ACI 318-02) and Commentary (ACI 318R-02)," American Concrete Institute, Farmington Hills, Michigan, USA, 2002.

2. ACI, Innovation Task Group 1, "Acceptance Criteria for Moment Frames Based on Structural Testing (ACI T1.1-01) and Commentary (ACI T1.1R-01)," American Concrete Institute, Farmington Hills, Michigan, USA, 2001.
3. Priestley, M. and Tao, J.R., "Seismic Response of Precast Prestressed Concrete Frames with Partially Debonded Tendons," *PCI Journal*, Precast/Prestressed Concrete Institute, v. 38, No. 1, January-February 1993, pp. 58-67.
4. Cheok, G. and Lew, H.S., "Model Precast Concrete Beam-to-Column Joints Subject to Cyclic Loading," *PCI Journal*, Precast/Prestressed Concrete Institute, v. 38, No. 4, July-August 1993, pp. 80-92.
5. Stanton, J., Stone, W., and Cheok, G., "A Hybrid Reinforced Precast Frame for Seismic Regions", *PCI Journal*, Precast/Prestressed Concrete Institute, v. 42, No. 2, March-April 1997, pp. 20-32.
6. El-Sheikh, M., Sause, R., Pessiki, S., and Lu, L.W., "Seismic Behavior and Design of Unbonded Post-Tensioned Precast Concrete Frames," *PCI Journal*, Precast/Prestressed Concrete Institute, v. 44, No. 3, May-June 1999, pp. 54-71.
7. El-Sheikh, M., Sause, R., Pessiki, S., and Lu, L.W., "Moment Rotation Behavior of Unbonded Post-Tensioned Precast Concrete Beam-Column Connections," *ACI Structural Journal*, American Concrete Institute, v. 97, No. 1, January-February 2000, pp. 122-131.
8. El-Sheikh, M., Sause, R., Pessiki, S., Lu, L.W., and Kurama, Y., "Seismic Analysis, Behavior, and Design of Unbonded Post-Tensioned Precast Moment Frames," Report No. EQ-97-02, Department of Civil and Environmental Engineering, Lehigh University, Bethlehem, PA, November 1997.
9. Priestley, M., Sritharan, S., Conley, J., and Pampanin, S., "Preliminary Results and Conclusions from the PRESSS Five-Story Precast Concrete Test Building," *PCI Journal*, Precast/Prestressed Concrete Institute, v. 44, No. 6, November-December 1999, pp. 42-67.
10. Stanton, J. and Nakaki, S., "Design Guidelines for Precast Concrete Seismic Structural Systems", Report No. PRESSS-01/03-09, Department of Civil Engineering, University of Washington, Seattle, Washington, February 2002.
11. Englekirk, R.E., "Design-Construction of The Paramount – A 39-Story Precast Prestressed Concrete Apartment Building," *PCI Journal*, Precast/Prestressed Concrete Institute, v. 47, No. 4, July-August 2002, pp. 56-71.
12. Christopoulos, C, Filiatrault, A., Uang, C-M., and Folz, B., "Post-tensioned Energy Dissipating Connections for Moment-Resisting Steel Frames," *Journal of Structural Engineering*, American Society of Civil Engineers, v. 128, No. 9, September 2002, pp. 1111-1120.
13. Morgen, B. and Kurama, Y., "Friction-Damped Unbonded Post-Tensioned Precast Concrete Moment Frame Structures: An Integrated Seismic Evaluation." *Structural Engineering Research Report #NDSE-04-02*, Department of Civil Engineering and Geological Sciences, University of Notre Dame, Notre Dame, IN, (expected 2004).
14. Morgen, B. and Kurama, Y., "A Cast-Steel Friction Damper for Post-Tensioned Precast Concrete Beam-to-Column Joints," *National Technical and Operating Conference, Session on Castings for Building*, Steel Founders' Society of America, Chicago, IL, November 6-8, 2003 (invited paper and presentation).
15. Morgen, B. and Kurama, Y., "A Friction Damper for Post-Tensioned Precast Concrete Beam-to-Column Joints," *PCI Journal*, Precast/Prestressed Concrete Institute (submitted 2003).
16. Grigorian, C., Yang, T., and Popov, E., "Slotted Bolted Connection Energy Dissipaters," *Earthquake Spectra*, Earthquake Engineering Research Institute, v. 9, No. 3, August 1993, pp. 491-504.
17. Way, D., "Friction-Damped Moment Resisting Frames," *Earthquake Spectra*, Earthquake Engineering Research Institute, v. 12, No. 3, August 1996, pp. 623-633.
18. Parkash, V., Powell, G., and Campbell, S., "DRAIN-2DX Base Program Description and User Guide; Version 1.10," Report No. UCB/SEMM-93/17, Department of Civil Engineering, University of California, Berkeley, California, November 1993.